



Computational Design of Custom-Fit PAP Masks

Yukun Lu^{a,c}, Yuhang Wang^{b,c}, Peng Song^{c,*}, Hang Siang Wong^d, Yingjuan Mok^d, Ligang Liu^a

^aUniversity of Science and Technology of China, China

^bNanjing University of Information Science and Technology, China

^cSingapore University of Technology and Design, Singapore

^dChangi General Hospital, Singapore

ARTICLE INFO

Article history:

Received June 21, 2024

Keywords:

Custom-fit PAP mask

Geometric modeling

Finite element analysis

Computational design

Digital fabrication

ABSTRACT

Positive airway pressure (PAP) therapy refers to sleep disordered breathing treatment that uses a stream of compressed air to support the airway during sleep. Even though the use of PAP therapy has been shown to be effective in improving the symptoms and quality of life, many patients are intolerant of the treatment due to poor mask fit. In this paper, our goal is to develop a computational approach for designing custom-fit PAP masks such that they can achieve better mask fit performance in terms of mask leakage and comfort. Our key observation is that a custom-fit PAP mask should fit a patient's face in its deformed state instead of in its rest state since the PAP mask cushion undergoes notable deformation before reaching an equilibrium state during PAP therapy. To this end, we compute the equilibrium state of a mask cushion using the finite element method, and quantitatively measure the leakage and comfort of the mask cushion in this state. We further optimize the mask cushion geometry to minimize the two measures while ensuring that the cushion can be easily fabricated with molding. We demonstrate the effectiveness of our computational approach on a variety of face models and different types of PAP masks. Experimental results on real subjects show that our designed custom-fit PAP masks are able to achieve better mask fit performance than a generic PAP mask and custom-fit PAP masks designed by a state-of-the-art approach.

© 2024 Elsevier B.V. All rights reserved.

1. Introduction

Sleep disordered breathing (SDB) refers to a wide spectrum of sleep-related respiratory conditions including obstructive sleep apnoea in which affected individuals experience recurrent airway collapse during sleep. SDB is estimated to affect 1 billion people worldwide [1]. Apart from causing daytime sleepiness and impaired quality of life, SDB has been associated with adverse cardiovascular outcomes. Positive Airway Pressure (PAP) therapy has been the first line treatment for SDB. With PAP therapy, the subject wears a PAP mask during sleep. A portable PAP

machine gently blows pressurized room air into the subject's upper airway through a tube connected to the PAP mask. This positive pressure airflow helps to keep the airway open, thus allowing normal breathing [2].

Even though the use of PAP therapy has been shown to be effective in improving the symptoms and quality of life, many patients are intolerant of PAP treatment due to *poor mask fit*. Currently, commercially available PAP masks (i.e., generic PAP masks) come in standard sizes, which are insufficient given the large variations in face shapes of patients. A poor mask fit can result in *mask leaks* and *patient discomfort*, leading to poor treatment tolerance and consequently poor compliance to PAP therapy. A PAP mask that does not fit well usually causes the air to leak, which reduces the efficiency of the therapy as the target

*Corresponding author.

E-mail address: peng_song@sutd.edu.sg (Peng Song).

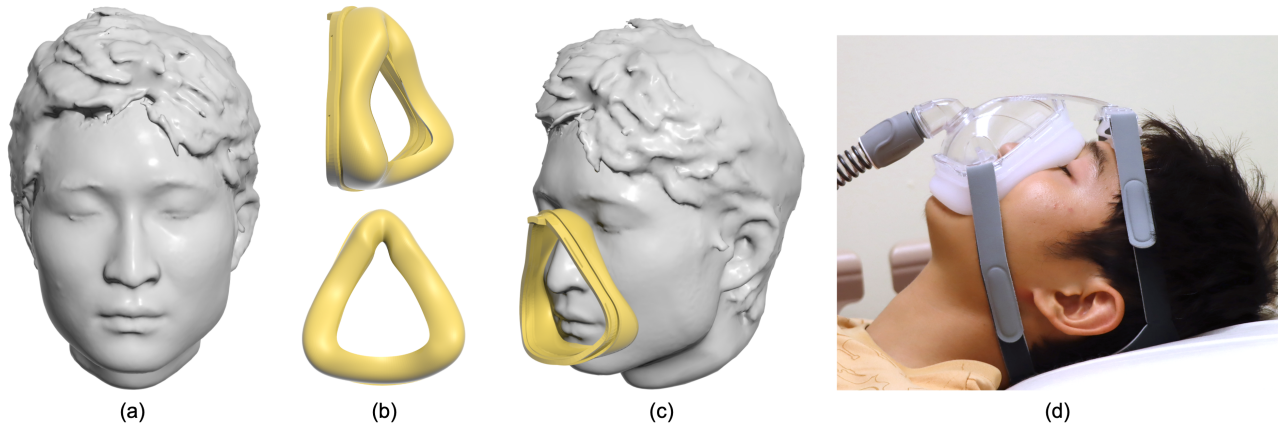


Fig. 1: Given (a) the scanned face model of a subject, we develop an optimization-based approach to design (b&c) a PAP mask cushion that fits the face model. (d) The designed mask cushion is fabricated and assembled with a generic mask frame to form a custom-fit PAP mask for practical use.

positive pressure within the upper airway cannot be maintained. Many patients tend to over tighten their mask straps in an attempt to compensate for ill-fitting masks that are leaking air, which could lead to discomfort and sometimes skin excoriation on the face.

To address the poor mask fit issue, a *custom-fit PAP mask* can be modeled and fabricated to fit the specific shape of a patient’s face. Since the mask cushion is the only part of the PAP mask that contacts a human face, the custom-fit PAP mask is generally modeled as an assembly of a *personalized mask cushion* and the frame of a generic PAP mask, where the personalized mask cushion is typically made with *soft silicone* material and the generic mask frame is made with hard plastic material. Existing works [3, 4] simply modeled the personalized mask cushion such that the cushion in its rest state exactly matches the static face model scanned for a patient. These works reported that their custom-fit mask is more comfortable than a generic mask yet there is no improvement on the air leakage.

Our key observation is that a custom-fit PAP mask should fit a scanned face model in its *deformed state* instead of in its *rest state* as the existing works [3, 4] do. This is because when a patient wears a mask for PAP therapy, the mask straps have to be tight enough to balance the pressurized air in the mask. The forces applied by the mask straps make the mask cushion undergo notable deformation before reaching an equilibrium state. A patient feels less leakage and comfortable only if the PAP mask in the equilibrium state fits the patient’s face well. However, designing such a custom-fit PAP mask is non-trivial since it requires computing the deformed shape of the mask cushion in the equilibrium state, evaluating the mask cushion in term of leakage and comfort in the equilibrium state, and optimizing the mask cushion’s geometry such that it can achieve better mask fit performance.

Given the face model of a subject, our goal is to develop a computational approach for designing and fabricating a personalized mask cushion that fits the subject’s face model, aiming to achieve better mask fit performance in terms of leakage and comfort. Our idea is to model and parameterize the mask cushion’s geometry as a swept surface (Section 3). This simple yet powerful geometry representation not only facilitates tetrahedralization of the cushion for the Finite Element Method (FEM)

simulation and makes the simulation differentiable but also defines an appropriate search space for our optimization-based design process. Specifically, we make the following technical contributions to address the above challenges:

- We compute an equilibrium state of the mask cushion by simulating the virtual mask-face fitting with FEM and propose quantitative measures on mask leakage and comfort for the cushion in this state (Section 4).
- We optimize the geometry of the mask cushion to minimize our measures on leakage and comfort computed from the FEM simulation while ensuring that the cushion can be easily fabricated by molding with silicone material (Section 5).

We demonstrate the effectiveness of our computational approach on face models with a variety of shapes and PAP masks of different types; see Figure 1 for an example. We conducted a user study to compare our designed custom-fit PAP masks with a generic PAP mask and the custom-fit PAP masks designed by a state-of-the-art approach [4], showing that our custom-fit masks have less air leakage and are more comfortable.

2. Related Work

Human-centric shape modeling. Objects in everyday use are shaped and given form based on their intended use and target user. In recent years, there has been a rising research interest in modeling man-made objects by making use of human poses and simulating the human-object interaction [5, 6, 7]. In particular, researchers utilized human sitting poses to model the geometric shape of rigid supporting surfaces to maximize the ergonomics of physically based contact between the surface and the human [8, 9, 10]. Instead of focusing on modeling man-made objects that are rigid, researchers also studied the problem of modeling custom-fit deformable garments based on 3D body scans of the intended wearer [11, 12, 13, 14, 15].

Head-related product design. Head-related products are designed for various purposes, including protection (e.g., protective helmets), enhancing sensory functioning (e.g., hearing aids), and information transfer (e.g., earphones). Traditionally, these

head-related products are designed by professionals and mass produced. However, due to variations in sizes and shapes of human heads, the mass-produced head-related products may not be suitable for a specific person. To address this limitation, researchers have developed methods to model customized head-related products, including hearing aid [16, 17], earphones [18], eyeglasses frame [19], and helmet [20]. Please refer to [21] for a recent survey on head-related product design. In this paper, we study computational techniques for designing a specific head-related product, mask.

Custom-fit mask design. A mask is an object normally worn on the face, typically for protection, disguise, medicine, or entertainment. Since standard masks may not fit well for everyone, customized design of masks is necessary. Researchers have studied customization of different types of masks, including pilot oxygen mask [22] and facial mask [23].

In particular, a number of research works focus on modeling and design of custom-fit PAP masks. Cheng et al. [24] developed customized mask cushions and compared the clinical performance of the customized cushion with the conventional one. Sela et al. [25] proposed a fully automatic approach for designing a personalized nasal mask interface that fits a facial depth scan. Wu et al. [3] developed an interactive tool to model custom-fit PAP masks and compared the custom-fit PAP masks with a generic mask in a user study. This work was later improved by Martelly et al. [4] to make the mask modeling and fabrication methodology more repeatable. Li et al. [26] developed an automatic pipeline to design a custom-fit PAP mask, including face scanning, processing, and mask modeling.

All the above existing works assume that the PAP mask cushion in its rest state exactly fits the human face model, and thus model the mask cushion by simply inverting the face shape. Moreover, they do not analyze the modeled mask cushion in terms of mask fit, not to mention optimizing the mask cushion geometry to improve the mask fit performance. We overcome these limitations by computing the deformed shape of the mask cushion in the virtual mask-face fitting using FEM, proposing quantitative measures on leakage and comfort of the deformed cushion, and optimizing the mask cushion's geometry to minimize the measures. We have compared our approach with a state-of-the-art approach [4] in a user study and shown that our designed custom-fit PAP masks has less air leakage and are more comfortable; see Section 6.

Designing deformable solids. Computational design of deformable solid objects with desired behavior have attracted attention from the computer graphics community. Some researchers achieve the deformable behavior by optimizing the object geometry, including the rest shape of an object that can deform to its target shape under external forces [27], cross-sectional profiles of rods in flexible meshes [28], and shell thickness of hollowed objects [29]. Other researchers designed objects with desired deformation behavior by optimizing the distribution of materials within the object [30, 31, 32]. Object geometry and material distribution can be jointly optimized to achieve desired deformation, e.g., when designing soft pneumatic objects [33]. In our paper, we also design a deformable solid (i.e., a personalized

cushion) for a PAP mask by optimizing its geometry, assuming evenly distributed (silicone) materials in the cushion. Different from the above works that optimize the object design to achieve prescribed deformable behavior, we optimize the cushion design of a PAP mask such that a patient feels comfortable and there is less air leakage when he/she wears the mask. This requires simulating the interaction between the cushion and the patient's face model (i.e., mask-face fitting) and evaluating comfort and air leakage based on the simulation result; see Section 4.

3. Geometry Modeling of Custom-fit Masks

We model a custom-fit PAP mask as an assembly of a personalized mask interface and the frame of a generic PAP mask. We choose a commercial PAP mask called the BMC F2 full face mask (middle size) as the generic mask since the interface of the BMC F2 mask can be easily replaced due to its mechanical connection with the mask frame; see Figure 2. We introduce our approach to modeling the geometry of the mask interface (Section 3.1) and the mask cushion (Section 3.2), where the mask cushion is the core component of the mask interface.

3.1. Modeling Mask Interface

The mask interface should be able to fit a subject's face and to join the BMC mask frame mechanically. To this end, we model the mask interface with two components; see Figure 3.

- *Cushion.* The cushion has a thin shell structure. Hence, we first model the cushion surface and then offset the surface along the normal direction for distance τ (τ is set as 3mm in our experiments) to get the shell geometry. Note that a

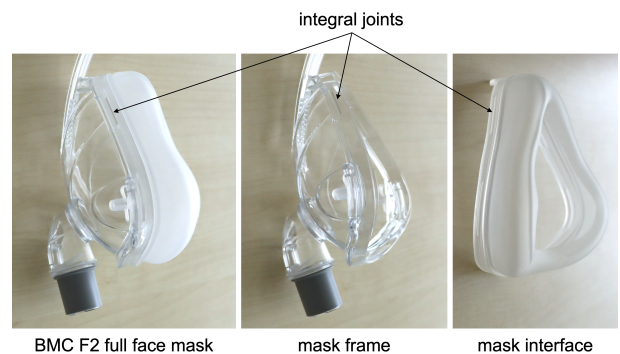


Fig. 2: (Left) The BMC F2 full face mask is an assembly of (middle) a mask frame and (right) a mask interface, where the mask frame and interface are connected mechanically based on the integral joints.

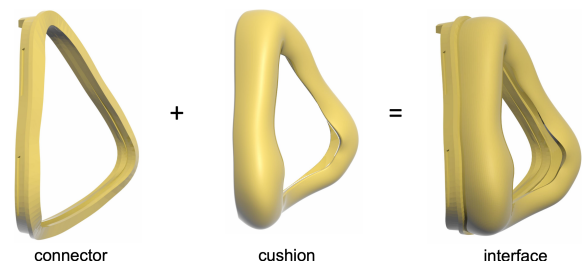


Fig. 3: We model a mask interface with two components: a connector for joining the BMC mask frame, and a mask cushion for fitting a subject's face.

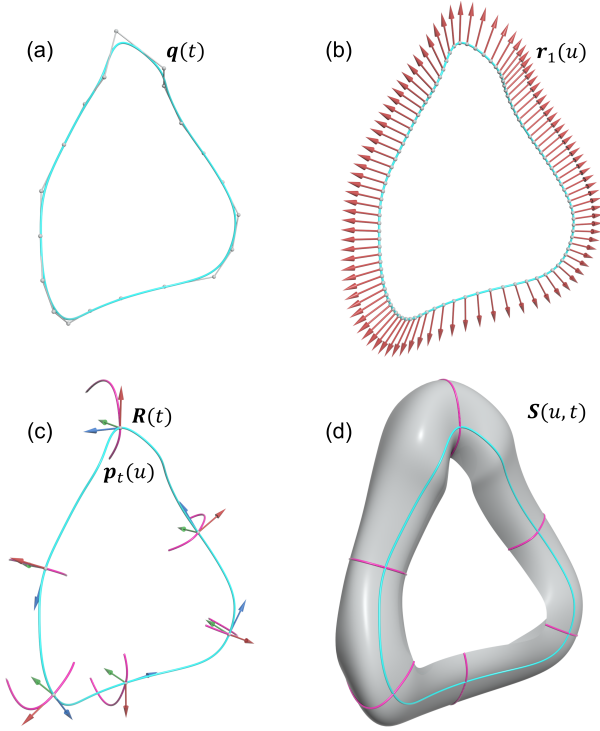


Fig. 4: Modeling the cushion surface using a swept surface: (a) a trajectory curve and its control polygon, (b) a set of sampled normals on the trajectory curve, (c) key profile curves defined in the XY plane of the local frame, and (d) the modeled cushion surface.

thickness of 3mm is not considered thin compared to the cushion thickness of commercial masks, and we choose this thickness for ease of fabrication. Section 3.2 provides details about cushion surface modeling.

- **Connector.** The connector of our mask interface always has the same geometry as that of the reconstructed BMC mask interface to enable mechanical joining between our modeled mask interface and the BMC mask frame.

3.2. Modeling Mask Cushion Surface

When wearing a PAP mask, the mask cushion contacts a subject's face and determines leakage and comfort of the mask. We choose to model the cushion surface using a parametric representation to ensure smooth geometry and reduce the design space. In particular, we model the cushion geometry using a *swept surface*; see Figure 4. A swept surface is generated by transforming 2D profile curves along a smooth rotation field defined on a 3D swept trajectory:

$$\begin{aligned} \mathbf{S}(u, t) &= \mathbf{q}(t) + \mathbf{R}(t) \mathbf{p}_t(u) \\ &= \begin{bmatrix} x(t) \\ y(t) \\ z(t) \end{bmatrix} + \begin{bmatrix} r_{11}(t) & r_{12}(t) & r_{13}(t) \\ r_{21}(t) & r_{22}(t) & r_{23}(t) \\ r_{31}(t) & r_{32}(t) & r_{33}(t) \end{bmatrix} \begin{bmatrix} \mathbf{p}_t^x(u) \\ \mathbf{p}_t^y(u) \\ 0 \end{bmatrix}, \end{aligned} \quad (1)$$

where $u \in [0, 1]$ and $t \in [0, 1]$ are parameters, $\mathbf{p}_t(u)$ is the 2D profile curve whose shape is varying with t , $\mathbf{q}(t)$ is the 3D swept trajectory curve that defines position of profile curve $\mathbf{p}_t(u)$ at t , and $\mathbf{R}(t)$ is the frame field represented as a 3×3 rotation matrix that defines orientation of profile curve $\mathbf{p}_t(u)$ at t .

Modeling trajectory curve $\mathbf{q}(t)$. We model the trajectory curve $\mathbf{q}(t)$ as a 3D periodic cubic B-spline curve:

$$\mathbf{q}(t) = \sum_{i=1}^n \mathbf{d}_i \hat{N}_i^4(t), \quad (2)$$

where n is the number of control points (typically set as 20 in our experiments), \mathbf{d}_i is the i th control point, and $\{\hat{N}_i^4\}_{i=1}^n$ is a set of cubic periodic B-spline functions. The B-spline curve is C^2 continuity, and has n different knots, where each knot has multiplicity 1; see Figure 4(a) for an example.

Modeling frame field $\mathbf{R}(t)$. The frame field can be written as $\mathbf{R}(t) = [\mathbf{r}_1(t), \mathbf{r}_2(t), \mathbf{r}_3(t)]$, where $\mathbf{r}_1(t)$, $\mathbf{r}_2(t)$, $\mathbf{r}_3(t)$ define the x -, y -, and z -axis of the local frame in the world space at parameter t , respectively; see the inset. One requirement of modeling the frame field $\mathbf{R}(t)$ is to minimize twisting of the local frames [34]. We observe that the trajectory curve $\mathbf{q}(t)$ is close to be parallel with the coronal plane of the human body when the mask is worn on the human face. The coronal plane, also known as the frontal plane, bisects the human body into anterior and posterior sections. Denote the normal of the coronal plane as \mathbf{n} . The tangent $\mathbf{q}'(t)$ of the trajectory curve $\mathbf{q}(t)$ should be close to be perpendicular to the normal \mathbf{n} . Thus, we use a simple method to compute the frame field $\mathbf{R}(t)$ with a slight twist:

$$\mathbf{r}_3(t) = \frac{\mathbf{P}_n \mathbf{q}'(t)}{\|\mathbf{P}_n \mathbf{q}'(t)\|}, \quad \mathbf{r}_2(t) = \mathbf{n}, \quad \mathbf{r}_1(t) = \mathbf{r}_2(t) \times \mathbf{r}_3(t), \quad (3)$$

where $\mathbf{P}_n = \mathbf{I} - \mathbf{nn}^T$ is a matrix that projects a vector onto the plane with normal \mathbf{n} ; see Figure 4(b) for an example. Self-intersection of the cushion surface may happen at high curvature points on the trajectory curve $\mathbf{q}(t)$. In this case, we resolve the self-intersection by using the frame relaxation approach in [16].

Modeling profile curves $\{\mathbf{p}_t(u)\}$. For each t , the 2D profile curve $\mathbf{p}_t(u)$ is defined in the XY plane of the local frame $\mathbf{R}(t)$. We require that each profile curve $\mathbf{p}_t(u)$ intersects with the trajectory curve $\mathbf{q}(t)$ in the 3D space. By this, the trajectory curve $\mathbf{q}(t)$ is on the cushion surface, and then we can initialize the trajectory curve $\mathbf{q}(t)$ easily based on the face shape. For each t , we model the profile curve $\mathbf{p}_t(u)$ as two quadratic Bézier curves joining G^1 smoothly at the origin of the local frame (i.e., point $\mathbf{q}(t)$):

$$\mathbf{p}_t(u) = \begin{cases} \mathbf{p}_t^1(1 - 2u), & (u, t) \in [0, 0.5] \times [0, 1], \\ \mathbf{p}_t^2(2u - 1), & (u, t) \in (0.5, 1] \times [0, 1], \end{cases} \quad (4)$$

where the Bézier curve \mathbf{p}_t^1 corresponds to the outer part of the cushion, and the Bézier curve \mathbf{p}_t^2 corresponds to the inner part of the cushion; see Figure 4(d) and 5. For PAP masks with more complex profile geometry, we can model the profile curves using Bézier curves with a higher order.

We denote the control points of the Bézier curve \mathbf{p}_t^j as $\{\mathbf{b}_i^j(t)\}$, $i \in \{0, 1, 2\}$ and $j \in \{1, 2\}$. For each profile curve $\mathbf{p}_t(u)$, $t \in [0, 1]$, the two Bézier curves \mathbf{p}_t^1 and \mathbf{p}_t^2 meet at the origin of the local frame, i.e., $\mathbf{b}_0^1(t) = \mathbf{b}_0^2(t) = \mathbf{b}_0(t) = \mathbf{0}$. Since we require that the profile curve is G^1 smooth at the origin, we represent $\mathbf{b}_1^1(t)$

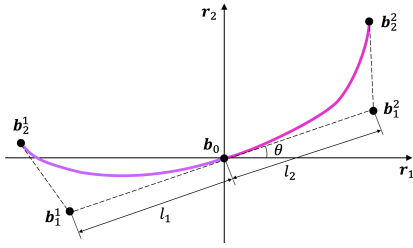


Fig. 5: The profile curve $\mathbf{p}_t(u)$ is modeled as two Bézier curves joining G^1 smoothly at the origin of the local frame.

and $\mathbf{b}_1^2(t)$ using the tangent angle $\theta(t)$ and two vector lengths $l_1(t) = \|\mathbf{b}_1^1(t) - \mathbf{b}_0(t)\|$ and $l_2(t) = \|\mathbf{b}_1^2(t) - \mathbf{b}_0(t)\|$ as:

$$\mathbf{b}_1^1 = \begin{bmatrix} -l_1 \cos(\theta) \\ -l_1 \sin(\theta) \end{bmatrix} + \mathbf{b}_0, \quad \mathbf{b}_1^2 = \begin{bmatrix} l_2 \cos(\theta) \\ l_2 \sin(\theta) \end{bmatrix} + \mathbf{b}_0. \quad (5)$$

To model the profile curves $\{\mathbf{p}_t(u)\}$, we only specify a few key profile curves for sampled parameters $t_1, t_2, \dots, t_K \in [0, 1)$. These key profile curves are independent with one another, and we typically choose $K = 15$ key profile curves in our experiments; see Figure 4(c&d) for an illustrative example with 6 key profile curves. All the other profile curves are obtained via interpolation of the key profile curves. We choose periodic C^2 cubic B-spline as the interpolant of the independent control points $\mathbf{b}_0(t)$, $\mathbf{b}_1^1(t)$ and $\mathbf{b}_2^2(t)$ and independent parameters $\theta(t)$, $l_1(t)$, and $l_2(t)$.

4. Evaluating Mask Cushion Surface

In this section, we evaluate a mask design in terms of air leakage and comfort by performing *virtual mask-face fitting*. We propose a quasi-static FEM model to efficiently simulate virtual mask-face fitting (Section 4.1). Based on the simulation result, we propose two measures to quantify the mask cushion in terms of leakage and comfort, respectively (Section 4.2).

4.1. Virtual Mask-Face Fitting

Accurately simulating the real mask-face fitting process is computationally expensive since it involves soft bodies (mask cushion and facial skin), rigid bodies (mask frame and facial bones), and fluid (compressed air). To make the simulation viable, we only simulate two core components: mask cushion and human face. Since the mask cushion (made with silicone) usually has a much larger deformation than the human face when a PAP mask is worn, we model the cushion as a deformable body and model the face as a rigid body. Friction between the mask cushion and the face is ignored in the simulation since it is relatively small compared with the contact normal force. In practice, it does not make sense to evaluate a mask design when the mask is not properly worn on the face. Hence, we assume that the mask-face alignment is known and fixed during the simulation; see supplementary material for details. We choose quasi-static FEM simulation for virtual mask-face fitting since we are only interested in the equilibrium state of the mask cushion rather than the procedure to arrive at that state.

Tetrahedralization of mask cushion. To support the FEM simulation, we generate a tetrahedral mesh for the cushion shell. Utilizing the swept surface model of the cushion surface, we can easily generate cushion tetrahedral mesh vertices by uniformly

sampling parameters $(u_i, t_j, h_k) \in [0, 1] \times [0, 1) \times [0, \tau]$, where τ is the cushion thickness. Note that the endpoints of each of the three intervals are always sampled. The vertices of the cushion shell in the rest state are represented as:

$$\bar{\mathbf{x}}_{ijk} = \mathbf{q}(t_j) + \mathbf{R}(t_j) (\mathbf{p}_{t_j}(u_i) - h_k \mathbf{n}_{t_j}(u_i)), \quad (6)$$

where $\mathbf{n}_t \in \mathbb{R}^3$ is the unit normal of the 2D profile curve \mathbf{p}_t in the 3D local frame, and its direction is consistent with that of the cushion surface normal. We use index (i, j, k) to refer to a vertex on the cushion tetrahedral mesh. In our experiments, the number of samples for (i, j, k) is $n_u = 11$, $n_t = 50$, $n_h = 2$, respectively. To determine the topology of the tetrahedral mesh, we first connect the sampled points to form a set of hexahedra and then divide each hexahedron into five tetrahedra [35]. We use first order tetrahedral element for the FEM simulation. Thus, nodes in the tetrahedral mesh are the same as the mesh's vertices. Compared with general tetrahedralization methods such as TetWild [36], our method has two advantages for mask cushion tetrahedralization: 1) vertices of the resulting tetrahedral mesh are differentiable with respect to the swept surface's control points; and 2) topology of the tetrahedral mesh are simple and fixed during the FEM simulation.

Quasi-static FEM simulation. Given the known mask-face alignment, there exists penetration between the mask cushion (in the rest state) and the face; see Figure 6 (top). During the quasi-static FEM simulation, we fix the face model and the cushion vertices that are attached to the connector. The goal of the FEM simulation is to compute the deformation of the mask cushion to resolve the mask-face penetration. The contact forces between the mask cushion and the face in the equilibrium state will be used to evaluate the mask cushion design in Section 4.2.

Denote $\mathbf{x}, \bar{\mathbf{x}} \in \mathbb{R}^{3N}$ as nodal positions in the cushion shell in the deformed and the rest state, respectively, where N is the number of nodes in the cushion shell. Furthermore, $\mathbf{x} = ((\mathbf{x}^c)^T, (\mathbf{x}^f)^T)^T$, where \mathbf{x}^c are the positions of nodes that are attached to the connector and fixed in the simulation and \mathbf{x}^f are the positions of the free nodes. The mask-face equilibrium state is obtained by minimizing the total potential energy:

$$\min_{\mathbf{x}^f} U(\mathbf{x}, \bar{\mathbf{x}}) + \omega_c C(\mathbf{x}^f), \quad (7)$$

where $U(\mathbf{x}, \bar{\mathbf{x}})$ is the cushion elastic potential energy, $C(\mathbf{x}^f)$ is the collision potential energy, and ω_c is the weight set as 1 in our experiments.

We use a linear elastic model for the cushion shell for simplicity. Although linear elasticity is not rotationally invariant, the cushion boundary remains fixed during the simulation, thus preventing introduction of any rigid motion. Note that the linear model can be replaced by a nonlinear model such as the Neo-Hookean model. The mask cushion is generally made with silicone and we set its material parameter as 1.11 MPa for Young's modulus and 0.49 for Poisson's ratio. Denote \mathbf{K} as the stiffness matrix [37]. The cushion elastic potential energy is represented as:

$$U(\mathbf{x}, \bar{\mathbf{x}}) = \frac{1}{2} (\mathbf{x} - \bar{\mathbf{x}})^T \mathbf{K} (\mathbf{x} - \bar{\mathbf{x}}). \quad (8)$$

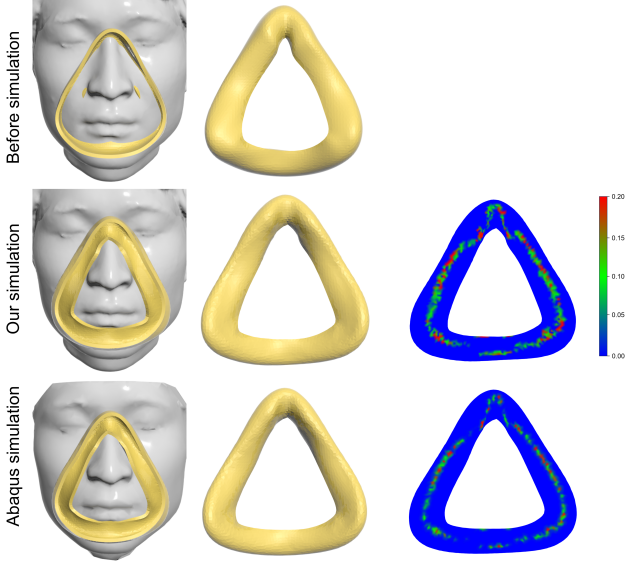


Fig. 6: (Top) For a known mask-face alignment, there is penetration between the mask cushion (in the rest state) and the human face. (Middle) We simulate the cushion shell deformation using quasi-static FEM to minimize the penetration, where the contact force magnitude in the deformed cushion surface is visualized on the right. (Bottom) We perform FEM simulation with Abaqus to evaluate our FEM model. The contact pressure in the two simulations is visualized on the right, which is very close to each other.

We use the signed distance field ϕ of the human face for defining the collision potential energy:

$$C(\mathbf{x}^f) = \sum_i (\min\{\phi(\mathbf{x}_i^f), 0\})^2. \quad (9)$$

The minimization problem in Equation 7 is solved using the L-BFGS method provided by ALGLIB library [38]. In order to justify our quasi-static FEM model, we perform mask-face fitting using the FEM simulation by the professional physical simulation software Abaqus [39]; see Figure 6. In Abaqus, we use Ogden hyperelastic model for the tetrahedral cushion, and model the human face as a rigid body. Initially, the face and mask have no interpenetration. Then we fix the position of the face model, and translate the cushion model to its position at the given mask-face alignment, during which the cushion is gradually deformed. We compare the cushion deformation result in Abaqus with ours and they are similar to each other. We measure the root-mean-squared error (RMSE) [8] between our computed vertex displacements and the vertex displacements computed in Abaqus, which is 0.0801. Note that we map the minimal displacement value to 0, and the maximal value to 1, with values in-between linearly interpolated. Consequently, the RMSE here is unitless. Moreover, the distribution of the nodal forces in the equilibrium state is also similar. We measure the RMSE between our computed contact force magnitudes and the contact force magnitudes computed in Abaqus, which is 0.0393. The experimental result shows that the deformed cushion shape and contact forces in the equilibrium state computed by our model are very close to those by Abaqus.

4.2. Evaluation Measures

We evaluate a mask cushion with two measures: air leakage measure and comfort measure, both of which are quantified based on the mask-face contact forces in the equilibrium state computed in the above FEM simulation.

Air leakage measure. In real mask-face fitting, a certain amount of contact pressure between the face and the mask is necessary to keep the compressed air flowing inside the PAP mask. Air leakage likely happens when the contact pressure is not evenly distributed across the mask cushion surface. We observe that there is no or little air leakage if the contact forces and areas are evenly distributed along the trajectory curve, where the contact area is identified as an area on the cushion surface that the contact force is not zero. So we propose to measure air leakage using the distribution of the contact force and area along the trajectory curve, respectively. To this end, we sum up the nodal force magnitudes and contact areas along each profile curve, respectively. Then, we compute the variance of the summed nodal force magnitudes and areas for all the profile curves along the trajectory curve, respectively, to measure the air leakage.

The force magnitude variance is defined as

$$V_{\text{force}} = \frac{1}{n_t} \sum_{j=1}^{n_t} \left(\sum_{i=2}^{n_u} \|\mathbf{f}_{ij}\|^2 - \frac{1}{n_t} \sum_{j=1}^{n_t} \sum_{i=2}^{n_u} \|\mathbf{f}_{ij}\|^2 \right)^2, \quad (10)$$

where $\mathbf{f}(\mathbf{x}, \bar{\mathbf{x}}) = -\nabla_{\mathbf{x}} U(\mathbf{x}, \bar{\mathbf{x}})$ is the vector of nodal forces on the deformed cushion and \mathbf{f}_{ij} is the nodal force at the node \mathbf{x}_{ij}^f on the cushion surface with index $(i, j, 1)$. Since nodes attached to the connector are fixed in the simulation, they are not included in Equation 10 (i.e., i starts from 2 instead of 1).

The contact area variance is defined as:

$$V_{\text{contact}} = \frac{1}{n_t} \sum_{j=1}^{n_t} \left(\sum_{i=2}^{n_u} A_{ij} s_{ij} - \frac{1}{n_t} \sum_{j=1}^{n_t} \sum_{i=2}^{n_u} A_{ij} s_{ij} \right)^2, \quad (11)$$

where A_{ij} is $\frac{1}{3}$ of total surface triangle areas of 1 ring neighbor of node \mathbf{x}_{ij}^f on the cushion surface, and s_{ij} is defined as $s_{ij} = \text{sign}(\|\mathbf{f}_{ij}\|)$ for identifying the contact area by filtering out nodes on the cushion surface with zero force magnitude. Note that $\text{sign}(\cdot)$ is a discontinuous function. To make s_{ij} suitable for the optimization-based design of the cushion surface in Section 5, we make s_{ij} differentiable using $s_{ij} = \tanh(k\|\mathbf{f}_{ij}\|^2)$, where k is a coefficient set as 100 in our experiments.

The air leakage measure is defined as:

$$E_{\text{leak}} = \lambda V_{\text{force}} + V_{\text{contact}}. \quad (12)$$

The choice of parameter λ depends on the cushion design, which is usually set as 111 in our experiments. We choose it so that the gradient norm of V_{force} is about the same scale as that of V_{contact} .

Comfort measure. In real mask-face fitting, discomfort occurs when the contact pressure on the face is too large. In our simulation, the pressure on the human face is caused by the elastic forces from the cushion surface. We measure comfort by approximating the average pressure on the human face using:

$$E_{\text{comf}} = \frac{\sum_{j=1}^{n_t} \sum_{i=2}^{n_u} \|\mathbf{f}_{ij}\|^2}{\left(\sum_{j=1}^{n_t} \sum_{i=2}^{n_u} A_{ij} s_{ij} \right)^2}, \quad (13)$$

5. Designing Mask Cushion Surface

Taking the geometry modeling in Section 3 and evaluation measures in Section 4 as a foundation, we propose an optimization-based approach to designing a personalized mask cushion for a subject whose face model is represented by a triangle mesh.

5.1. Problem Formulation

We formulate the design of a mask cushion surface for a subject as an optimization problem.

Search space. Our goal is to find the geometry of the mask cushion surface that fits a subject's face. Recall that the mask cushion surface is modeled as a swept surface represented by a trajectory curve and a few key profile curves (see again Figure 4). Hence, the search space of our problem is the control points of the trajectory curve \mathbf{q} and the parameters of the key profile curves $\{\mathbf{p}_i\}, i = 1, \dots, K$.

Objective function. Our design problem is formulated as minimizing the following objective function:

$$E = \omega_1 E_{\text{leak}} + \omega_2 E_{\text{comf}} + \omega_3 E_{\text{regu}}, \quad (14)$$

where E_{leak} is the leakage measure defined in Equation 12, E_{comf} is the comfort measure defined in Equation 13, E_{regu} is the regularization term that aims to maintain a cushion-like shape for the swept surface, ω_1, ω_2 and ω_3 are weights that are typically set as 1.8×10^3 , 1.11×10^{-4} , and 1×10^{-3} in our experiments, respectively. E_{leak} and E_{comf} are functions of $\bar{\mathbf{x}}, \mathbf{x}$, which are vertices in the tetrahedral mesh of the mask cushion in the rest and deformed state, respectively. In particular, $\bar{\mathbf{x}}$ is represented by the design variables via Equation 6, while \mathbf{x} is computed by running the quasi-static FEM simulation in Section 4.1. E_{regu} regularizes the cushion surface shape by constraining the key profile curves' length and shape, as well as distance between adjacent key profile curves; see the supplementary material for details. Note that E_{leak} becomes 0 and E_{comf} becomes undefined when there is no contact between the face and the cushion. Our regularization term aims to prevent occurring of such an undesired situation.

Constraints. The mask cushion shape has to satisfy the following constraints.

1. *Convex profile curves.* Most PAP masks on the market, including the BMC masks, have cushions with convex profile curves; see again Figure 2. This is likely because convex profile curves potentially lead to continuous mask-face contact, increasing comfort of the mask. We require convexity for our key profile curves. This is achieved by requiring the control polygon of each profile curve to be convex:

$$\det(\mathbf{b}_0(t_i) - \mathbf{b}_1^1(t_i), \mathbf{b}_2^1(t_i) - \mathbf{b}_1^1(t_i)) > 0, \quad i = 1, \dots, K, \quad (15)$$

$$\det(\mathbf{b}_2^2(t_i) - \mathbf{b}_1^2(t_i), \mathbf{b}_0(t_i) - \mathbf{b}_1^2(t_i)) > 0, \quad i = 1, \dots, K. \quad (16)$$

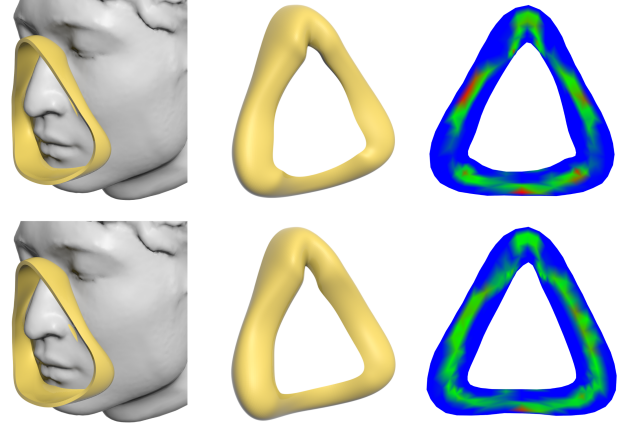


Fig. 7: The mask cushion surface (top) before and (bottom) after our optimization, and the FEM analysis result is shown on the right. The color map visualizes contact pressure values in range $[0, 2.2]$.

2. *Fixed cushion boundary.* The cushion with optimized shape should always match the connector with fixed shape to form the mask interface; see again Figure 3. To this end, the outer boundary curve of the cushion surface $\mathbf{S}(u, t)$ should interpolate the extracted curve $\mathbf{c}(y)$, $y \in [0, 1)$ on the mask connector for m samples ($m = 150$ in our experiments). This constraint is formulated as for each sample $z_i \in [0, 1)$, $i = 1, \dots, m$,

$$\mathbf{S}(0, z_i) = \mathbf{c}(y_i), \quad \exists y_i \in [0, 1). \quad (17)$$
3. *Collision-free tetrahedral mesh of the cushion shell.* To ensure a valid FEM simulation, collision among tetrahedra should be avoided in the tetrahedral mesh of the cushion shell. This is achieved by requiring that the volume of each tetrahedron in the tetrahedral cushion shell in the rest state should be positive [40]. This constraint also helps to avoid self-intersection in the cushion surface.
4. *Height-field cushion surface.* We fabricate the designed mask interface using molding with silicone material; see the supplementary material for details. To reduce the number of mold pieces for ease of fabrication, we require that the inner part of the cushion surface $I = \{\mathbf{S}(u, t) | (u, t) \in [0, 0.5] \times [0, 1)\}$ is a height field in the de-molding direction (same as the human face coronal plane normal \mathbf{n}). Hence, for any two points $A, B \in I$, ($A \neq B$), we have $\mathbf{P}_n(A) \neq \mathbf{P}_n(B)$, where $\mathbf{P}_n = \mathbf{I} - \mathbf{nn}^T$ projects a 3D point onto a plane with normal \mathbf{n} .

5.2. Optimization Solver

Initialization. It is important to find a good initial cushion surface for optimization. Our initialization is based on the scanned BMC mask cushion surface. There are two steps for the initialization. The first step is to find the trajectory curve, and the second step is to find the key profile curves. We extract a centerline curve on the scanned BMC mask cushion surface, project the centerline curve (represented as a polyline) on the human face and fit the projected polyline curve with a periodic cubic B-spline curve in Equation 2 to obtain the initial trajectory curve. For the key profile curve initialization, we first obtain each key

profile curve from the BMC mask cushion surface represented by a polyline, and then fit the polyline with the two Bézier curves in Equation 4 to obtain the corresponding initial key profile curve. Figure 7 (top) shows the cushion surface obtained from this initialization.

Optimization. In the optimization stage, we fix the trajectory curve as well as the local frames and only optimize the key profile curves. By this, the fixed cushion boundary constraint can be easily satisfied by fixing the control point $\mathbf{b}_2^1(t)$ of each key profile curve. To allow optimizing the key profile curves with a higher degree of freedom, we do not require the control point $\mathbf{b}_0(t) = \mathbf{0}$ for all t in the local frame; see again Figure 5.

In the optimization, we handle constraints by using the barrier function and quadratic penalty function. Especially, we use barrier function for the collision-free tetrahedral mesh and height-field cushion surface constraints, because these are hard constraint that must be satisfied. In case the initial cushion surface does not satisfy the collision-free tetrahedral mesh constraint, we resolve it by decreasing the key profile curve maximum curvature. We find our initial cushion surface generally satisfies the height-field constraint, since the inner part of the BMC mask cushion surface is a height field. The convexity constraint is handled by a penalty term using the quadratic penalty function.

We use gradient-descent with backtracking line search for optimization, and precondition the gradient by using BFGS matrix as an approximation of the Hessian matrix. We can derive the Jacobian matrix $\frac{\partial \mathbf{x}^f}{\partial \mathbf{x}}$ by using the condition $\mathbf{f}_f(\mathbf{x}, \bar{\mathbf{x}}) = \mathbf{0}$ at the quasi-static equilibrium state, where \mathbf{f}_f is denoted as the total nodal force exerted on the free nodes. Then, the gradient of the objective function ∇E can be computed using the adjoint method [41]. Figure 7 (bottom) shows one cushion surface optimized by our algorithm. By running our optimization on the mask cushion surface, the leakage measure is decreased from 0.0026 to 0.00066 and the comfort measure is decreased from 18.45 to 11.96. Please refer to the supplementary material for details about our solver.

6. Results

We implement our approach in C++ and use OpenMesh, libigl, and Eigen for geometry computing and ALGLIB for optimization. We execute our computational tool on a laptop PC with a 2.5GHz CPU and 16GB memory. Table 1 shows statistics of the results shown in the paper. It shows that the air leakage measure E_{leak} and comfort measure E_{comf} are significantly improved by our optimization on the cushion surface. The human face models used in our experiments were obtained through 3D scanning of real subjects (Figure 1, 8 (top), 10, and 11), provided by the FaceScape dataset [42] (Figure 9), and downloaded from online 3D model websites (Figure 8 (middle) and (bottom)).

Custom-fit PAP mask for different face shapes. Figure 8 shows that our approach allows designing a custom-fit PAP mask for subjects with a variety of face shapes. Due to the large variation of the face shapes, the generic BMC F2 mask does not fit each of them very well. In contrast, our designed custom-fit mask is

Table 1: Statistics and timings of results shown in the paper. We report the number of triangles in the face model, number of triangles in the mask interface, number of tetrahedra in the cushion shell, E_{leak} of the initial cushion surface, E_{comf} of the initial cushion surface, E_{leak} of the optimized cushion surface, E_{comf} of the optimized cushion surface, and time to solve the optimization-based design problem.

Figure		face #tri	cushion #tri	cushion #tet	initial E_{leak}	initial E_{comf}	optimized E_{leak}	optimized E_{comf}	Optim. (min)
1		60.8K	133.5K	2.5K	0.00260	18.45	0.00066	11.96	36.2
	top	91.4K	135.2K	2.5K	0.00120	18.14	0.00029	12.93	88.2
8	mid	35.1K	129.8K	2.5K	0.00191	26.41	0.00050	21.27	85.6
	bot	83.7K	137.3K	2.5K	0.00182	17.85	0.00081	12.56	183.8
9		79.8K			0.00109	16.78	0.00046	14.56	
	lef	80.3K	130.7K	2.5K	0.00060	18.13	0.00037	16.84	294.3
		80.8K			0.00071	17.85	0.00039	14.57	
	mid	79.8K	135.1K	2.5K	0.00095	20.12	0.00024	14.88	146.5
10	top	60.1K	61.2K	2.5K	0.00021	13.43	0.00005	7.28	30.1
	mid	60.1K	61.2K	2.5K	0.01726	10.05	0.00038	2.13	48.6
	bot	60.1K	61.2K	4.0K	0.00076	13.96	0.00027	7.50	55.2
11(c)	lef	265.0K	132.1K	2.5K	0.00269	30.53	0.00094	25.04	152.3
	rig	265.3K	130.1K	2.5K	0.00083	23.04	0.00029	18.43	84.1

able to achieve better performance than the BMC mask in terms of leakage and comfort for all the subjects. One interesting observation is that the BMC mask fits the first subject better than the others. This is likely because the BMC mask is designed according to the 3D anthropometric data of a population’s faces and the first subject’s face is closer to the representative face of the population. This experiment demonstrates that our approach is particularly useful for designing a custom-fit mask for subjects whose face is far from the representative face of the population since generic PAP masks do not fit their faces well.

Custom-fit PAP mask for multiple face expressions. Our approach assumes that a subject’s face is static when wearing the mask. However, a subject may have different face expressions when wearing the mask; e.g., the mouth can be either open or closed. Our approach can be generalized to design a custom-fit mask for subjects with multiple face expressions when wearing a mask. This is achieved by modifying the objective function in our optimization-based design. In detail, we perform virtual mask-face fitting for each face expression, and use their combined evaluation measures as the metric to evaluate a cushion candidate. Weights can be specified to each face expression and used for the linear combination of the evaluation measures. Figure 9 shows that a custom-fit mask designed for three typical face expressions achieves better mask fit performance than the custom-fit mask designed only for face expression #1 as well as the BMF F2 mask.

Custom-fit PAP mask of different types. We show that our approach allows designing PAP masks of different types, not limited to BMC F2 full face mask. PAP masks can be classified into three types: nasal mask that only covers the nose, full face mask that covers the nose and mouth, and total face mask that covers the whole face. For the same subject, we used our approach to design a personalized cushion for a nasal mask, a full face

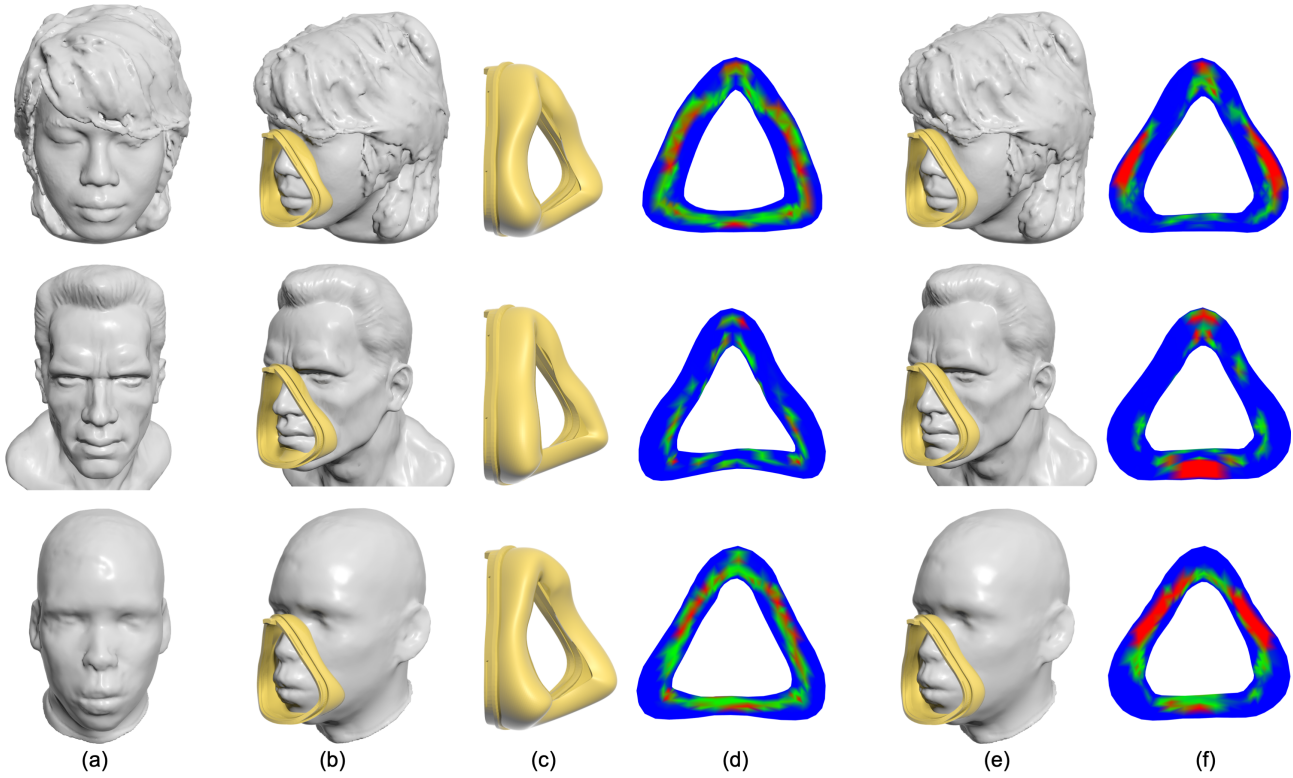


Fig. 8: Our approach allows designing (b&c) a custom-fit PAP mask for (a) subjects with a variety of face shapes, achieving better mask fit performance than (e) the BMC F2 mask for each subject. (d) The contact forces of our custom-fit PAP masks are more evenly distributed across the cushion trajectory curve than (f) those of the BMC F2 mask (i.e., less leakage), and the contact forces of our custom-fit PAP masks have smaller magnitudes than those of the BMC F2 mask (i.e., more comfortable). The color map visualizes contact pressure values in range $[0, 1.5]$.

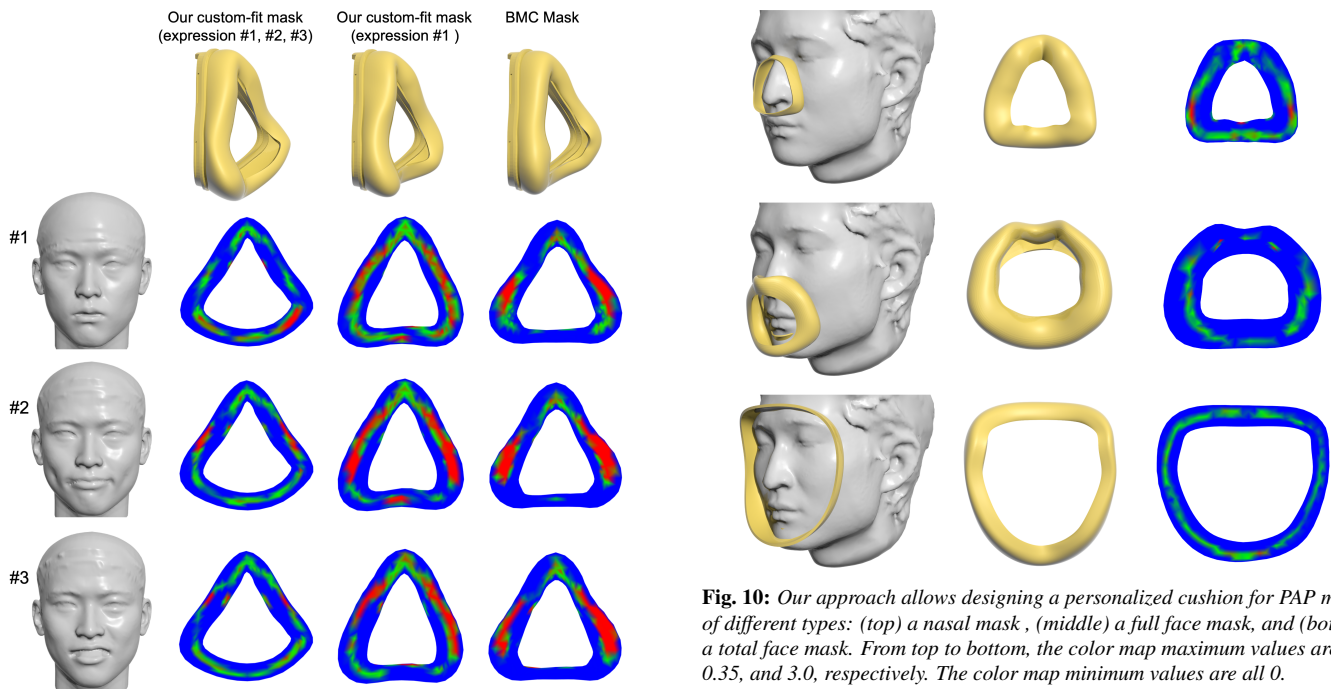


Fig. 9: Our approach allows designing a custom-fit mask for a subject with three different expressions [42], achieving better mask fit performance than a custom-fit mask designed only for expression #1 as well as the BMC F2 mask. The color map visualizes contact pressure values in range $[0, 1.5]$.

mask (with a different form from the BMC F2 mask), and a total face mask; see Figure 10. For each mask type, our designed

Fig. 10: Our approach allows designing a personalized cushion for PAP masks of different types: (top) a nasal mask, (middle) a full face mask, and (bottom) a total face mask. From top to bottom, the color map maximum values are 0.7, 0.35, and 3.0, respectively. The color map minimum values are all 0.

personalized cushion achieves good mask fit performance in terms of leakage and comfort.

User study on real subjects. The purpose of this user study on healthy real subjects is to gather feedback about the air leakage

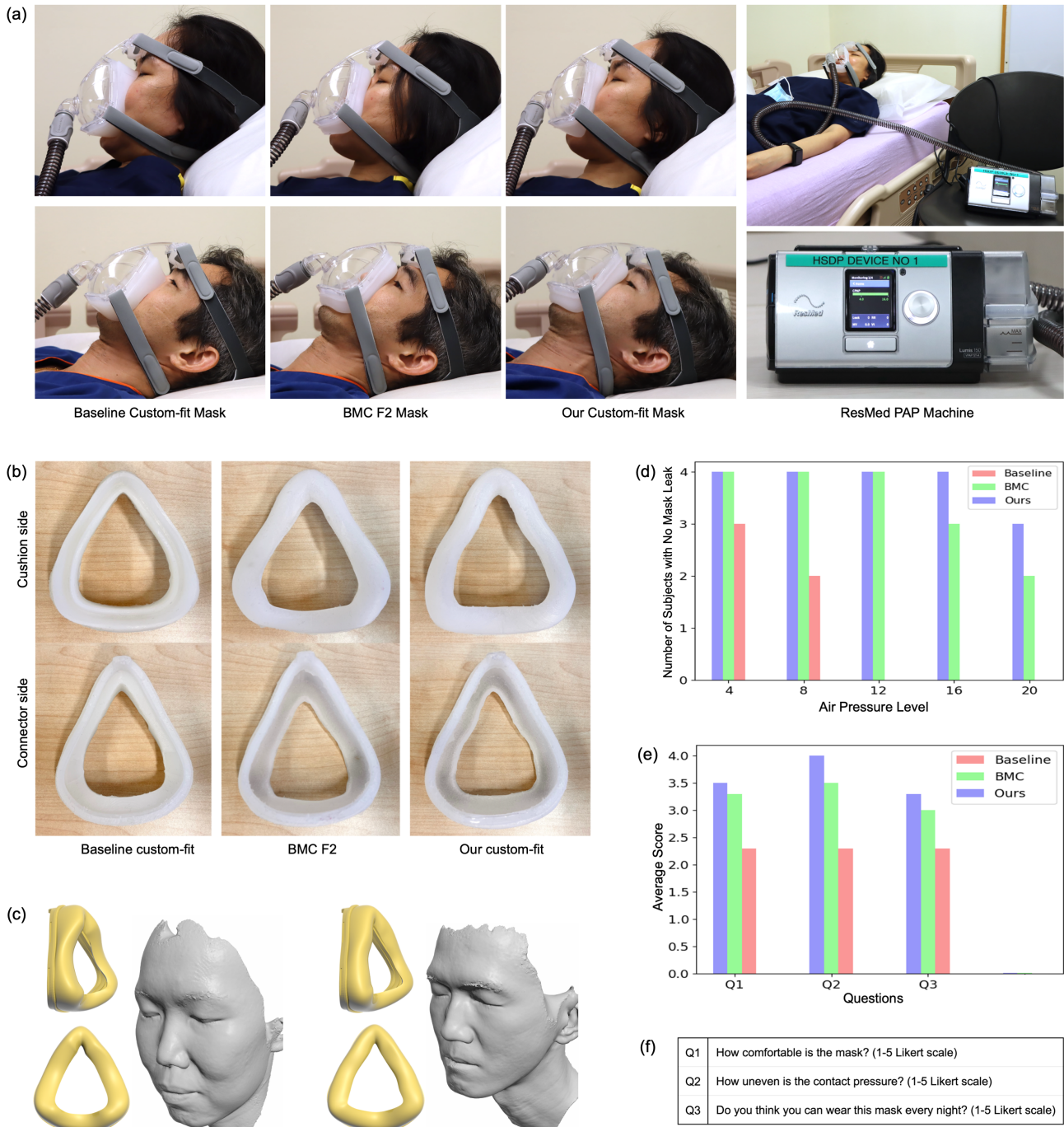


Fig. 11: (a) A user study on two real subjects who wore the baseline custom-fit mask, BMC F2 mask, and our custom-fit mask, respectively. The user study setting is shown on the right, where a subject is lying on the bed and wearing a PAP mask that is connected to a ResMed PAP machine. (b) Three cushions (designed for the male subject) are fabricated with silicone and used in our user study. (c) Face models of the two subjects and the custom-fit mask designed for each of them using our approach. (d) Air leakage statistics in our user study, reporting the number of subjects with no air leakage for each mask and each air pressure level. (e) Summary of the four users' answers to Q1 - Q3 in (f) our post-study questionnaire.

and comfort with our custom-fit mask. Four healthy subjects (3 male, 1 female; age 23 - 46) participated in the study, among which two are respiratory sleep physicians. For each subject, we first scan his/her face using the handheld EinScan H Scanner to obtain a mesh model of the face; see Figure 1(a), 8(top) and 11(c) for the face models of the subjects. Next, we use our computational approach to design a personalized mask cushion that fits the subject's face model. We fabricate the designed

cushion with silicone by casting silicone into a 3-piece mold modeled according to the cushion's shape. Thanks to the height-field constraint in our optimization, only three mold pieces are enough to fabricate the cushion with freeform shape; see the supplementary for details. In this study, we compare our custom-fit mask with the BMC F2 mask as well as a baseline custom-fit mask designed using the approach in [4], which simply models the cushion (with a concave U-shaped profile) by inverting

the subject's face shape. We fabricate the three cushions with silicone material using the same method; see Figure 11(b) for examples. Please watch the accompanying video for demos.

During the study, a subject tries each of the three masks without knowing the mask type; see Figure 11(a). The procedure of the study is as follows. First, the subject wears the mask in a lying position, during which a respiratory sleep physician adjusts the mask such that it is comfortable to wear and have a good seal. Next, the mask is connected to a PAP machine. Initially, the PAP machine is set to deliver a continuous positive airway pressure (CPAP) of 4 cmH₂O, during which the physician further adjusts the mask alignment until no air leakage. Then, the CPAP pressure of the machine is increased to 8, 12, 16, and 20 cmH₂O, during which the air leakage data (provided by the machine) is recorded for each air pressure level. The subject is asked to fill a questionnaire at the end of the study; see Figure 11(f).

Figure 11(d) provides the recorded air leakage data for the four subjects. For each mask and each air pressure level, the table provides the number of subjects that do not report air leakage using the mask under the air pressure level. The user study result shows that our custom-fit mask is significantly better than the baseline mask for all air pressure levels and better than the BMC F2 mask for 16 and 20 cmH₂O pressure levels. Figure 11(e) summarizes the subjects' feedback to the questionnaire. All the participants think that our custom-fit mask is better than the baseline mask and the BMC F2 mask in terms of comfort and even contact pressure.

7. Conclusion

This paper studies computational design and fabrication of custom-fit PAP masks that have less air leakage and are more comfortable to wear, aiming to improve a patient's compliance to PAP therapy. The mask interface is a core component of a custom-fit PAP mask, determining the mask's air leakage and comfort. We propose a family of computational techniques to model, evaluate, and design a personalized mask interface that fits a subject's face model when the PAP mask is in use, and integrate these techniques into a computational tool that greatly simplifies the design process. We have employed our computational tool to design a personalized mask interface for subjects with a variety of face shapes, and fabricated some of them by molding with silicone material. Our user study on real subjects confirms that our custom-fit PAP mask can achieve better mask fit performance than a generic PAP mask as well as custom-fit PAP masks designed by an existing approach.

Limitations and future work. Our work has several limitations that open up directions for future research. First, in the current virtual mask-face fitting, we assume that the human face is rigid to simplify the simulation process. In the future, we plan to model the human face as a deformable body, possibly with rigid bones inside. We also plan to simulate compressed air within the mask such that the simulation result can be closer to the real counterpart, resulting in a more accurate air leakage measure. Second, the current user study is conducted on healthy subjects, including two physicians, showing that our custom-fit mask can improve the PAP therapy. Further clinical study on patients with

sleep disordered breathing would be an important future work. Third, this paper focuses on computational design of PAP masks. We hope our approach is able to inspire new computational approaches to design and fabricate personalized cushions for different kinds of face-related products such as oxygen masks, swimming goggles, and VR/AR headsets.

Acknowledgement

We thank the reviewers for their valuable comments, Pengyun Qiu for participating in the user study, Thileepan Stalin and Pablo Valdivia y Alvarado for providing advice and facilities on fabricating mask interfaces with silicone. We would also like to thank the Changi General Hospital Office of Innovation and Clinical Trials Research Unit for their support in this project. This work was supported by the CGH – SUTD HealthTech Innovation Fund (CGH-SUTD-HTIF-2021-001), the MOE Academic Research Fund Tier 2 Grant (MOE-T2EP20222-0008), Singapore, and the National Natural Science Foundation of China (62025207).

References

- [1] Benjafield, AV, Ayas, NT, Eastwood, PR, Heinzer, R, Ip, MSM, Morrell, MJ, et al. Estimation of the global prevalence and burden of obstructive sleep apnoea: A literature-based analysis. *The Lancet Respiratory Medicine* 2019;7(8):687–698. [https://doi.org/10.1016/S2213-2600\(19\)30198-5](https://doi.org/10.1016/S2213-2600(19)30198-5).
- [2] Kakkar, RK, Berry, RB. Positive airway pressure treatment for obstructive sleep apnea. *CHEST* 2007;132(3):1057–1072. <https://doi.org/10.1378/chest.06-2432>.
- [3] Wu, YY, Acharya, D, Xu, C, Cheng, B, Rana, S, Shimada, K. Custom-fit three-dimensional-printed bipap mask to improve compliance in patients requiring long-term noninvasive ventilatory support. *Journal of Medical Devices* 2018;12(3):031003:1–031003:8. <https://doi.org/10.1115/1.4040187>.
- [4] Martelly, E, Rana, S, Shimada, K. Design and fabrication of custom-fit BiPAP and CPAP masks using three-dimensional imaging and three-dimensional printing techniques. *Journal of Medical Devices* 2021;15(2):024502:1–024502:7. <https://doi.org/10.1115/1.4049981>.
- [5] Kim, VG, Chaudhuri, S, Guibas, L, Funkhouser, T. Shape2Pose: Human-centric shape analysis. *ACM Trans on Graph (SIGGRAPH)* 2014;33(4):120:1–120:12. <https://doi.org/10.1145/2601097.2601117>.
- [6] Zheng, Y, Liu, H, Dorsey, J, Mitra, NJ. Ergonomics-inspired reshaping and exploration of collections of models. *IEEE Trans Vis & Comp Graphics* 2016;22(6):1732–1744. <https://doi.org/10.1109/TVCG.2015.2448084>.
- [7] Fu, Q, Chen, X, Su, X, Fu, H. Pose-inspired shape synthesis and functional hybrid. *IEEE Trans Vis & Comp Graphics* 2017;23(12):2574–2585. <https://doi.org/10.1109/TVCG.2017.2739159>.
- [8] Leimer, K, Birsak, M, Rist, F, Musialski, P. Sit & Relax: Interactive design of body-supporting surfaces. *Comp Graph Forum (Pacific Graphics)* 2018;37(7):349–359. <https://doi.org/10.1111/cgf.13573>.
- [9] Leimer, K, Winkler, A, Ohrhallinger, S, Musialski, P. Pose to Seat: Automated design of body-supporting surfaces. *Comp Aided Geom Des* 2020;79:101855:1–101855:16. <https://doi.org/10.1016/j.cagd.2020.101855>.
- [10] Zhao, D, Li, Y, Chaudhuri, S, Langlois, T, Barbič, J. ERGOBOSS: Ergonomic optimization of body-supporting surfaces. *IEEE Trans Vis & Comp Graphics* 2022;28(12):4032–4047. <https://doi.org/10.1109/TVCG.2021.3112127>.
- [11] Wang, CCL, Tang, K. Pattern computation for compression garment by a physical/geometric approach. *Computer-Aided Design* 2010;42(2):78–86. <https://doi.org/10.1016/j.cad.2009.02.018>.
- [12] Montes, J, Thomaszewski, B, Mudur, S, Popa, T. Computational design of skintight clothing. *ACM Trans on Graph (SIGGRAPH)* 2020;39(4):105:1–105:12. <https://doi.org/10.1145/3386569.3392477>.

- [13] Liu, Z, Han, X, Zhang, Y, Chen, X, Lai, YK, Doubrovski, EL, et al. Knitting 4D garments with elasticity controlled for body motion. *ACM Trans on Graph (SIGGRAPH)* 2021;40(4):62:1–62:16. <https://doi.org/10.1145/3450626.3459868>.
- [14] Vechev, V, Zarate, J, Thomaszewski, B, Hilliges, O. Computational design of kinesthetic garments. *Comp Graph Forum (Eurographics)* 2022;41(2):535–546. <https://doi.org/10.1111/cgf.14492>.
- [15] Wolff, K, Herholz, P, Ziegler, V, Link, F, Brügel, N, Sorkine-Hornung, O. Designing personalized garments with body movement. *Comp Graph Forum* 2023;42(1):180–194. <https://doi.org/10.1111/cgf.14728>.
- [16] Azernikov, S. Computer aided design of ventilation tubes for customized hearing aid devices. *Computer-Aided Design* 2010;42(2):87–94. <https://doi.org/10.1016/j.cad.2009.02.015>.
- [17] Sickel, K, Baloch, S, Melkisetoglu, R, Bubnik, V, Azernikov, S, Fang, T. Toward automation in hearing aid design. *Computer-Aided Design* 2011;43(12):1793–1802. <https://doi.org/10.1016/j.cad.2011.06.005>.
- [18] Liu, K, Wang, H, Liu, Q, Chen, Q. A web-based application for TWS earphone design and fit evaluation. In: *Proc. International Conference on Human-Computer Interaction*. 2022, p. 157–167. https://doi.org/10.1007/978-3-031-05906-3_12.
- [19] Chu, CH, Wang, J, Wang, JB, Luh, YP. 3D parametric human face modeling for personalized product design: Eyeglasses frame design case. *Advanced Engineering Informatics* 2017;32:202–223. <https://doi.org/10.1016/j.aei.2017.03.001>.
- [20] Zhang, J, Luximon, Y, Shah, P, Zhou, K, Li, P. Customize My Helmet: A novel algorithmic approach based on 3D head prediction. *Computer-Aided Design* 2022;150:103271:1–103271:10. <https://doi.org/10.1016/j.cad.2022.103271>.
- [21] Zhang, J, Luximon, Y, Shah, P, Li, P. 3D statistical head modeling for face/head-related product design: A state-of-the-art review. *Computer-Aided Design* 2023;159:103483:1–103483:24. <https://doi.org/10.1016/j.cad.2023.103483>.
- [22] Lee, W, Jung, D, Park, S, Kim, H, You, H. Development of a virtual fit analysis method for an ergonomic design of pilot oxygen mask. *Applied Sciences* 2021;11(12):5332:1–5332:15. <https://doi.org/10.3390/app11125332>.
- [23] Kwon, YJ, Kim, JG, Lee, W. A framework for effective face-mask contact modeling based on finite element analysis for custom design of a facial mask. *PLoS ONE* 2022;17(7):e0270092:1–e0270092:19. <https://doi.org/10.1371/journal.pone.0270092>.
- [24] Cheng, YL, Hsu, DY, Lee, HC, Bien, MY. Clinical verification of patients with obstructive sleep apnea provided with a customized cushion for continuous positive airway pressure. *The Journal of Prosthetic Dentistry* 2015;113(1):29–34. <https://doi.org/10.1016/j.prosdent.2014.01.030>.
- [25] Sela, M, Toledo, N, Honen, Y, Kimmel, R. Customized facial constant positive air pressure (CPAP) masks. 2016. *ArXiv preprint arXiv:1609.07049* <https://doi.org/10.48550/arXiv.1609.07049>.
- [26] Li, S, Ploumpis, S, Zafeiriou, S, Myant, C. Design automation for mass customisation via additive manufacture: A case study on continuous positive airway pressure mask. In: *Proc. International Design Engineering Technical Conferences and Computers and Information in Engineering Conference*. 2020, p. V11AT11A026:1–V11AT11A026:7. <https://doi.org/10.1115/DETC2020-22316>.
- [27] Chen, X, Zheng, C, Xu, W, Zhou, K. An asymptotic numerical method for inverse elastic shape design. *ACM Trans on Graph (SIGGRAPH)* 2014;33(4):95:1–95:11. <https://doi.org/10.1145/2601097.2601189>.
- [28] Pérez, J, Thomaszewski, B, Coros, S, Bickel, B, Canabal, JA, Sumner, R, et al. Design and fabrication of flexible rod meshes. *ACM Trans on Graph (SIGGRAPH)* 2015;34(4):138:1–138:12. <https://doi.org/10.1145/2766998>.
- [29] Zhang, X, Le, X, Wu, Z, Whiting, E, Wang, CC. Data-driven bending elasticity design by shell thickness. *Comp Graph Forum* 2016;35(5):157–166. <https://doi.org/10.1111/cgf.12972>.
- [30] Bickel, B, Bäcker, M, Otaduy, MA, Lee, HR, Pfister, H, Gross, M, et al. Design and fabrication of materials with desired deformation behavior. *ACM Trans on Graph (SIGGRAPH)* 2010;29(4):63:1–63:10. <https://doi.org/10.1145/1778765.1778800>.
- [31] Skouras, M, Thomaszewski, B, Coros, S, Bickel, B, Gross, M. Computational design of actuated deformable characters. *ACM Trans on Graph (SIGGRAPH)* 2013;32(4):82:1–82:10. <https://doi.org/10.1145/2461912.2461979>.
- [32] Zehnder, J, Knoop, E, Bäcker, M, Thomaszewski, B. MetaSilicone: Design and fabrication of composite silicone with desired mechanical properties. *ACM Trans on Graph (SIGGRAPH Asia)* 2017;36(6):240:1–240:13. <https://doi.org/10.1145/3130800.3130881>.
- [33] Ma, LK, Zhang, Y, Liu, Y, Zhou, K, Tong, X. Computational design and fabrication of soft pneumatic objects with desired deformations. *ACM Trans on Graph (SIGGRAPH Asia)* 2017;36(6):239:1–239:12. <https://doi.org/10.1145/3130800.3130850>.
- [34] Wang, W, Jüttler, B, Zheng, D, Liu, Y. Computation of rotation minimizing frames. *ACM Trans on Graph* 2008;27(1):2:1–2:18. <https://doi.org/10.1145/1330511.1330513>.
- [35] Hacon, D, Tomei, C. Tetrahedral decompositions of hexahedral meshes. *European Journal of Combinatorics* 1989;10(5):435–443. [https://doi.org/10.1016/S0195-6698\(89\)80017-4](https://doi.org/10.1016/S0195-6698(89)80017-4).
- [36] Hu, Y, Zhou, Q, Gao, X, Jacobson, A, Zorin, D, Panozzo, D. Tetrahedral meshing in the wild. *ACM Trans on Graph (SIGGRAPH)* 2018;37(4):60:1–60:14. <https://doi.org/10.1145/3197517.3201353>.
- [37] Logan, DL. *A First Course in the Finite Element Method (Enhanced 6th Edition)*. Cengage Learning; 2022.
- [38] ALGLIB LTD, . Alglib library. 2023. <https://www.alglib.net/>.
- [39] Smith, M. *Abaqus/standard user's manual, version 6.9*. 2009. <https://research.manchester.ac.uk/en/publications/abaqusstandard-users-manual-version-69>.
- [40] Müller, M, Chentanez, N, Kim, TY, Macklin, M. Air meshes for robust collision handling. *ACM Trans on Graph (SIGGRAPH)* 2015;34(4):133:1–133:9. <https://doi.org/10.1145/2766907>.
- [41] Wang, H. Rule-free sewing pattern adjustment with precision and efficiency. *ACM Trans on Graph (SIGGRAPH)* 2018;37(4):53:1–53:13. <https://doi.org/10.1145/3197517.3201320>.
- [42] Yang, H, Zhu, H, Wang, Y, Huang, M, Shen, Q, Yang, R, et al. FaceScape: a large-scale high quality 3D face dataset and detailed riggable 3D face prediction. In: *Proc. IEEE Conf. on Comp. Vis. and Pat. Rec.* 2020, p. 601–610. <https://doi.org/10.1109/CVPR42600.2020.00068>.